Citation for final published version:

Ortmann, John Elliott, Nookala, Nishant, He, Qian , Gao, Lingyuan, Lin, Chungwei, Posadas, Agham, Borisevich, Albina Y., Belkin, Mikhail A. and Demkov, Alexander A. 2018. Quantum confinement in oxide heterostructures: room-temperature intersubband absorption in SrTiO3/LaAlO3 multiple quantum wells. ACS Nano 12 (8) , pp. 7682-7689. 10.1021/acsnano.8b01293

Publishers page: http://dx.doi.org/10.1021/acsnano.8b01293

Quantum Confinement in Oxide Heterostructures: Room-Temperature Intersubband Absorption in SrTiO3/LaAlO3 Multiple Quantum Wells

John Elliott Ortmann, Nishant Nookala, Qian He, Lingyuan Gao, Chungwei Lin,
Agham Posadas, Albina Y. Borisevich, Mikhail A. Belkin, and Alexander A. Demkov

Just Accepted

“Just Accepted” manuscripts have been peer-reviewed and accepted for publication. They are posted online prior to technical editing, formatting for publication and author proofing. The American Chemical Society provides “Just Accepted” as a service to the research community to expedite the dissemination of scientific material as soon as possible after acceptance. “Just Accepted” manuscripts appear in full in PDF format accompanied by an HTML abstract. “Just Accepted” manuscripts have been fully peer reviewed, but should not be considered the official version of record. They are citable by the Digital Object Identifier (DOI®). “Just Accepted” is an optional service offered to authors. Therefore, the “Just Accepted” Web site may not include all articles that will be published in the journal. After a manuscript is technically edited and formatted, it will be removed from the “Just Accepted” Web site and published as an ASAP article. Note that technical editing may introduce minor changes to the manuscript text and/or graphics which could affect content, and all legal disclaimers and ethical guidelines that apply to the journal pertain. ACS cannot be held responsible for errors or consequences arising from the use of information contained in these “Just Accepted” manuscripts.

Quantum Confinement in Oxide Heterostructures:
Room-Temperature Intersubband Absorption in $SrTiO_3/LaAlO_3$ Multiple Quantum Wells

John Elliott Ortmann[1], Nishant Nookala[2,3], Qian He[4], Lingyuan Gao[1], Chungwei Lin[1,5], Agham Posadas[1], Albina Y. Borisevich[4], Mikhail A. Belkin[2,3], and Alexander A. Demkov[1*]

[1]Department of Physics, The University of Texas, Austin, TX 78712, USA

[2]Department of Electrical and Computer Engineering, The University of Texas, Austin 78712, TX, USA

[3]Microelectronics Research Center, The University of Texas at Austin, Austin, TX 78758, USA

[4]The Materials Science and Technology Division, Oak Ridge National Laboratory, Oak Ridge, TN 37831, USA

[5]Mitsubishi Electric Research Laboratories, Cambridge, MA 02139, USA

Abstract

The Si-compatibility of perovskite heterostructures offers the intriguing possibility of producing oxide-based quantum well (QW) optoelectronic devices for use in Si photonics. While the $SrTiO_3/LaAlO_3$ (STO/LAO) system has been studied extensively in the hopes of using the interfacial 2-dimensional electron gas in Si-integrated electronics, the potential to exploit its giant 2.4 eV conduction band offset in oxide-based QW optoelectronic devices has so far been largely ignored. Here, we demonstrate room-temperature intersubband absorption in STO/LAO QW heterostructures at energies on the order of hundreds of meV, including at energies approaching the critically important telecom wavelength of 1.55 μm. We demonstrate the ability to control the absorption energy by changing the width of the STO well layers by a single unit cell and present theory showing good agreement with experiment. A detailed structural and chemical analysis of the samples *via* scanning transmission electron microscopy (STEM) and electron energy loss spectroscopy (EELS) is presented. This work represents an important proof-of-concept for the use of transition metal oxide QWs in Si-compatible optoelectronic devices.

Keywords: Transition metal oxides, intersubband transitions, quantum wells, oxide-oxide interface, heterostructure, thin films

A plethora of emergent phenomena in transition metal oxide (TMO) thin film heterostructures has been observed in the last several years thanks to the precise control of their structural and chemical properties afforded by pulsed laser deposition (PLD) and molecular beam epitaxy (MBE). Many of the emergent phenomena in TMO heterostructures have no bulk analogues and

---

[*] demkov@physics.utexas.edu

occur exclusively in artificial material systems whose parent compounds do not share similar properties. For example, two-dimensional superconductivity has been observed at the interface of $SrTiO_3$ (STO) and $LaAlO_3$ (LAO),[1–3] materials which are both band insulators. Furthermore, oxide heterostructures have demonstrated magnetism at the interface of two otherwise nonmagnetic compounds,[1,2,4–6] conductivity at the interface of wide band-gap insulators,[7] and several different forms of electronic reconstruction.[8–13] These unexpected physical properties are fascinating from the perspective of fundamental physics while also promising to advance the state-of-the-art of thin film devices. In particular, the Si- and Ge-compatibility of perovskite TMO films and heterostructures[14–16] makes these materials intriguing for use in technological applications, such as Si-integrated electronics[17–19] and Si photonics.[20]

In addition to exotic phenomena arising from the correlated physics of *d*-electrons, TMO heterostructures offer an impressive range of highly controllable band alignments[21] and can be engineered with large band offsets, suggesting extreme quantum confinement.[22] The combination of large and controllable band offsets with the possible interplay between quantum confined particles and correlated phenomena in TMO QW heterostructures could lead to the fabrication of QW devices with advanced functionalities. For example, by incorporating ferroelectric $BaTiO_3$ into QW heterostructures one could engineer structures whose quantum-confined states experience a Stark shift in response to internal fields from ferroelectric domains, allowing for ferroelectric switching of absorption energy and offering an extra degree of freedom as compared to externally-biased GaAs QWs.[23] Similarly, $GdTiO_3$/STO heterostructures have shown proximity-induced ferromagnetism in the STO QWs,[24,25] possibly allowing for enhanced magnetic field control of confined energy levels. Finally, heterostructures grown with piezoelectric $PbZr_yTi_{1-y}O_3$ could allow for bias-induced strain-tuning of electronic transitions during device operation, functionality not present in traditional QW devices. The fabrication of heterostructures featuring $PbTiO_3$ has in fact already been demonstrated[26–28] and exotic dielectric properties have been observed in improper ferroelectric STO/$PbTiO_3$ heterostructures.[29,30] The fact that such TMO heterostructures can also be readily integrated on Si (001) makes them not only fundamentally interesting but also technologically relevant, particularly in the field of Si photonics. While we offer these example systems for the fabrication of TMO QW devices, the literature offers many examples of interesting phenomena in TMO heterostructures,[9,13] a large number of which can host confined charge carriers if engineered properly.

Despite their promise, many challenges, such as the technical difficulty of growing the sufficiently thick, high-quality heterostructures necessary for device applications, have slowed the practical demonstration of TMO-based QW devices. So far, the only successful demonstration of mid-infrared intersubband absorption in TMO heterostructures was reported in ZnO/ZnMgO multiple QWs.[31] Unfortunately, in contrast to most perovskite TMO heterostructures, this materials system cannot be integrated directly onto Si (001), limiting its technological significance. Perhaps the most famous of TMO heterostructures, the STO/LAO system boasts a conduction band offset of 2.34 eV,[32] making it a prime candidate for hosting confined electrons. This is to be contrasted with offsets of a meager few tenths of eV in commonly-used GaAs/$Ga_{1-x}Al_xAs$ QW heterostructures.[33] Such a small offset severely limits the operating energy range of traditional GaAs-based QW devices relying on intersubband transitions. In addition to its large conduction band offset, recent measurements in STO/LAO QW heterostructures[32] have demonstrated the Burstein-Moss effect, confirming the presence of electronic confinement and further suggesting the feasibility of using the STO/LAO system in the construction of TMO-based QW devices. However, before such devices can be reliably constructed, two major challenges must be overcome. First, the growth of thick STO/LAO heterostructures must be perfected, as previous studies have observed progressive roughening of successive layers.[34] Secondly, control of optically modulated intersubband transitions must be demonstrated in STO/LAO heterostructures, preferably at room-temperature, before any real attempts at device fabrication can hope to succeed. In this report, we demonstrate the ability to overcome both obstacles.

We grow STO/LAO short-period QW heterostructures with up to eighty well/barrier periods on LAO substrates and demonstrate room-temperature intersubband absorption on the order of hundreds of meV. In particular, we demonstrate absorption at energies nearing the critically important telecom wavelength of 1.55 μm. We further show the ability to control the intersubband absorption energy *via* QW width modulation of a single unit cell. Our Fourier-transform infrared (FTIR) spectroscopy results for heterostructures with three-, four-, and five-unit cell (u.c.) wells clearly demonstrate absorption at approximately 650 meV, 540 meV, and 350 meV, respectively, in good agreement with tight binding and density functional theory calculations. Additionally, we describe our solution to the problem of growth through a detailed structural and chemical analysis of the samples *via* scanning transmission electron microscopy (STEM) and electron energy loss spectroscopy (EELS), demonstrating the excellent crystal quality with which these heterostructures can be fabricated. Through statistical analysis of STEM images, we quantify the interfacial roughness in these heterostructures to be less than one u.c. on average. While the heterostructures described in this report are grown on LAO substrates and have not yet been integrated with silicon, the demonstration of room-temperature infrared intersubband absorption in STO/LAO QW heterostructures, whose energy can be modulated by atomically controlled changes in QW width, represents an important proof-of-concept toward the realization of TMO optoelectronic devices compatible with silicon photonics. The structural quality and optical properties of such heterostructures integrated on Si (001) have not yet been investigated and are important topics of study for future reports.

Results and Discussion

Growth: Atomic-scale control of structure and chemical composition. In Figure 1a, we present a general schematic of the QW samples studied. The samples were grown on LAO substrates, leading to compressively strained STO wells reinforced by unstrained LAO barriers. La serves as an electron donor in STO when substituting for Sr,[35,36] thereby introducing electrons into the STO conduction band. These electrons can then be optically modulated between confined states within the STO QW, as demonstrated in the “Room-temperature infrared intersubband absorption” section below. We confirm the successful doping of our QWs *via* room-temperature Hall measurements presented in Supporting Information Section 4 and in Figure S8.

As the samples used in this study are significantly thicker than previously-reported STO/LAO heterostructures,[5,7,12,32,34] great care must be taken to ensure the crystalline quality remains high throughout the entire thickness of the sample. To this end, we present a wide-field, Z-contrast STEM image and corresponding EELS mapping of a $[(La_{0.01}Sr_{0.99}TiO_3)_6/(LaAlO_3)_7]_{40}$ QW heterostructure in Figure 1b. The wide-field view, covering the entire thickness of the sample, confirms excellent periodicity is maintained throughout the sample. The bright LAO bands and dark STO bands are clearly distinguishable from one another over the entire sample thickness. Such separation of STO well and LAO barrier layers is crucial for the demonstration of intersubband transitions, as electronic confinement in the wells relies on clear structural and chemical separation between well and barrier layers. The clear chemical separation between layers is also verified by the Ti and La EELS mapping in Figure 1b. Taken together, these measurements demonstrate the successful growth and atomic-scale control of thick STO/LAO heterostructures, a prerequisite for our study. XRD measurements showing clear superlattice peaks out to 4th-order are presented in Supporting Information Figure S3.

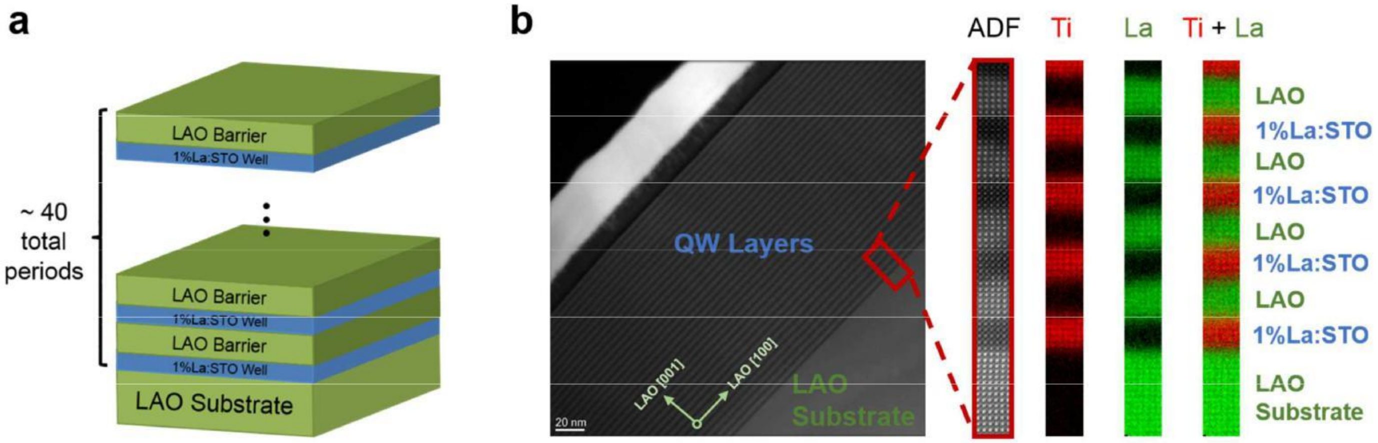

Figure 1. (**a**) Schematic of the general design of our QW heterostructures. The STO well layers vary in thickness from three to six u.c. while the LAO barrier layers are kept at a constant thickness of seven u.c. to ensure the electronic wave functions in adjacent wells remain uncoupled. (**b**) Large-field STEM image over the entire thickness of a six-u.c. well heterostructure, demonstrating clearly separated STO well and LAO barrier layers. A magnified view of a small region of the heterostructure is also presented, showing an annular dark-field (ADF) image as well as corresponding La and Ti EELS spectra.

Statistical analysis of interfacial roughness. Just as the overall structural quality of our STO/LAO heterostructures is critically important for the successful observation of intersubband absorption, so too is the interfacial quality. As our heterostructures have extremely thin well layers, minor variations in QW width in the form of interfacial roughness can have a significant impact on the energy eigenvalues. Furthermore, QW interfacial quality can greatly influence the degree of confinement in QWs[37] and the spectral line shape,[38,39] with rougher interfaces leading to broader absorption peaks. Thus, before we can reasonably expect to observe intersubband absorption, we must ensure the interfaces are of low roughness. This is especially important in the STO/LAO system, as significant structural distortions at both the *n*- and *p*-type STO/LAO interfaces have been reported.[34,40–43]

To study the interfacial quality of our samples in detail and ensure they are of suitable quality for the observation of intersubband absorption, we have carried out a statistical analysis of interfacial roughness using STEM intensity mapping of a 40-period, nominally four-u.c. QW heterostructure (Figure 2). The STEM image in Figure 2a shows excellent long-range periodicity of the heterostructure over the visible 11 well/barrier periods. No misfit dislocations are present in this relatively large (~50x50 nm^2) field of view, demonstrating no apparent degradation of crystal quality with increasing thickness. The clear difference in intensity between Sr and La allows us to evaluate the statistics of the QW widths as detected from the images. We can compute integrated intensity for every La or Sr cation column in the image in Fig. 2a, producing an intensity map where each pixel is a u.c. (Supporting Information Figure S4). By using an appropriate threshold, we convert the intensity map into a binary image, where unit cells with Sr are represented by black pixels and those with La are represented by white pixels (Figure 2b). We then compute a width in unit cells for every u.c.-wide region of every well, giving us 1452 measurements from this image area. From this analysis, we find an average well width of 4.32 ± 0.63 u.c. for the sample in Figure 2, in good agreement with the nominal well width of 4 u.c. More details of our analysis can be found in Section 3 of the Supporting Information.

From the binary map presented in Figure 2b, we can further get a sense of the interfacial quality by examining the roughness of the top (*n*-type) and bottom (*p*-type) interfaces of each STO well. We can evaluate the roughness in multiple ways: by computing the deviation of the well boundary from a flat line contour (integral roughness), or by counting the number of interface steps per unit length. The integral roughness measurements are presented in Figure 2c, separately for well bottoms (black) and tops (red). Averaging the standard deviations of each interface over the visible 11 well/barrier periods, we find a mean deviation of 0.24 ± 0.25 u.c. for the *n*-type interface and 0.34 ± 0.26 u.c. for the *p*-type interface. Differential roughness gives us 0.31 ± 0.12 steps/nm for the *p*-type interface and 0.36 ± 0.28 steps/nm for the *n*-type. While our thresholding approach does not consider possible differences in the compositional spread, it should still accurately reveal the contour of the interface. Notably, our analysis indicates the interfacial roughness is symmetric between the *n*- and *p*-type interfaces in our samples, in contrast with many experimental and theoretical reports on STO/LAO heterostructures.[32,34,42] This anomalous feature could be related to the doping in our QWs, as additional charge is required at the *n*-type interface to avoid the so-called polar catastrophe in LAO.[7,44] Most importantly for the present study, however, both interfaces show remarkably low interfacial roughness, suggesting the observation of intersubband absorption is feasible in our samples.

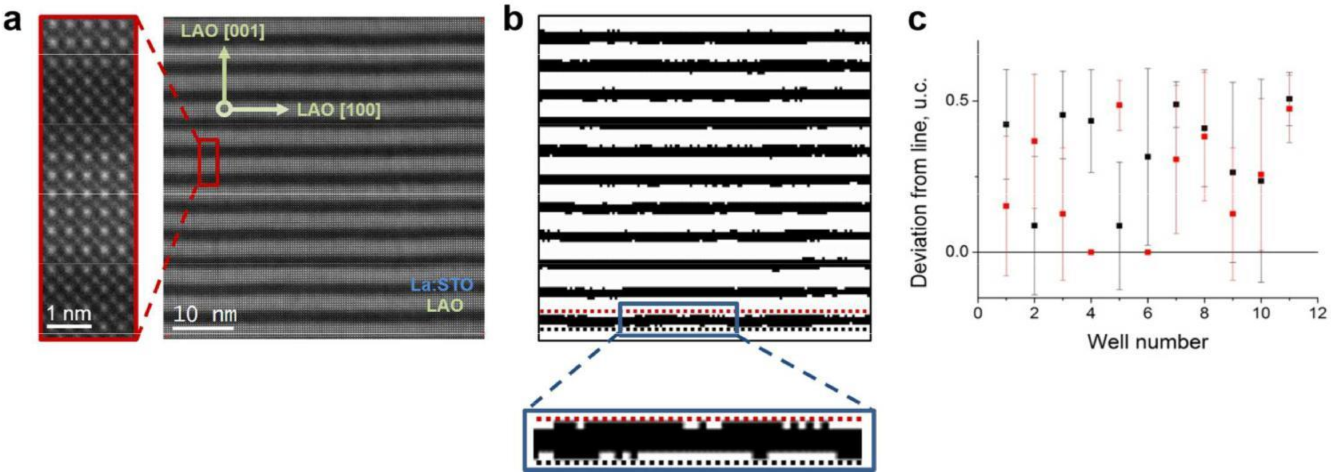

Figure 2. **(a)** Z-contrast images (large scale and close-up) of a nominally $[(La_{0.01}Sr_{0.99}TiO_3)_4/(LaAlO_3)_7]_{40}$ QW heterostructure showing uniform periodicity and lack of extended defects. (**b**) Binary (0 = well (Sr), 1 = barrier (La)) image generated by thresholding of A-site (La and Sr) intensity mapping of the large-scale image in **a**. The zoom-in shows the deviations from a perfectly smooth interface, as plotted in panel **c**. **(c)** Average deviation of the well edges from a horizontal line for the well tops (red) and well bottoms (black) computed from the binary image in **b**. The apparent lattice spacing variation in LAO in the left panel of 2a is caused by a charging effect due to the highly insulating nature of LAO.

Room-temperature infrared intersubband absorption. Having established the excellent structural and interfacial quality of our heterostructures, we turn our attention to absorption. In Figure 3a, we present FTIR spectroscopy results for STO/LAO QW heterostructures with three-, four-, and five-u.c. wells, clearly showing absorption peaks at energies specific to each measured structure. The six-u.c. well absorption is not included here as its energy is too low to be measured with the present setup. By utilizing the polarization selection rule for intersubband transitions,[45–47] we are able to isolate absorptions that only occur for a given polarization of the excitation source (see Supporting Information). This procedure, demonstrated schematically in Figure 3b, removes the ambiguity as to the origin of the observed absorptions, as more common absorption mechanisms, such as excitation of phonons, should not adhere to the polarization selection rule of intersubband absorption. Besides the polarization dependence, the energies of the observed absorptions in our QW heterostructures are significantly higher than the phonon energies in either STO or LAO,[48,49] further suggesting the observed absorptions are due to intersubband transitions in the QWs.

As can be seen from Figure 3a, the absorption energies scale appropriately with the QW width. This result not only agrees qualitatively with general quantum theory, it also agrees with recent reports on electronic confinement in the STO conduction band of STO/LAO QW heterostructures.[32] We also observe a decrease in absorption peak amplitude that scales with decreasing QW width. This is consistent with a greater population of the ground state in wider wells. In fact, the amplitude of the absorption peak from the three u.c.-well sample (inset Figure 3a) is approaching the lower resolution limit of the current setup. This can be attributed to a combination of a smaller ground state population in this sample as compared to the other samples, leading to a decreased peak amplitude, as well as broadening from interfacial roughness. In a sample with three u.c. QWs, small variations in well width will lead to a greater change in energy eigenvalues than comparable width variations in samples with wider wells, leading to significant broadening of the absorption peak. As a certain amount of interfacial roughness is unavoidable in these systems owing to thermodynamic constraints,[41] observing intersubband absorption in wells thinner than 3 u.c. will be challenging. Nevertheless, the observation of intersubband absorption at 650 meV in the three u.c.-well sample hints at the possibility of reaching the important telecom energy of 1.55 μm (= 800 meV) in perovskite TMO QWs. By designing heterostructures whose constituent materials feature a smaller effective mass[35,50] than that of STO, it should be within the realm of possibility to reach such energies in TMO QW heterostructures.

In Figure 3c, we plot the results of tight binding (TB) calculations for three-, four-, and five-u.c. STO wells for comparison with experiment. TB has been employed previously to compute the electronic band structure and corresponding photon absorption spectrum in bulk TMOs and similar TMO QW heterostructures.[51] Here, we calculate the frequency-dependent dielectric function of STO QWs and plot the imaginary part of the dielectric function, corresponding to absorption in the heterostructures. The calculated spectra agree well with the experimental spectra in several respects. First, the calculated and measured spectra agree relatively well in terms of the absolute absorption energies. While there are slight discrepancies between theory and experiment, these can easily be attributed to small variations in well width of the measured heterostructures. Secondly, the relative spacing between absorptions from wells of different widths agrees between TB calculations and experiment. Finally, the relative peak amplitudes are consistent between TB calculations and experiment, corresponding to a reduction in ground state electron population for narrower QWs.

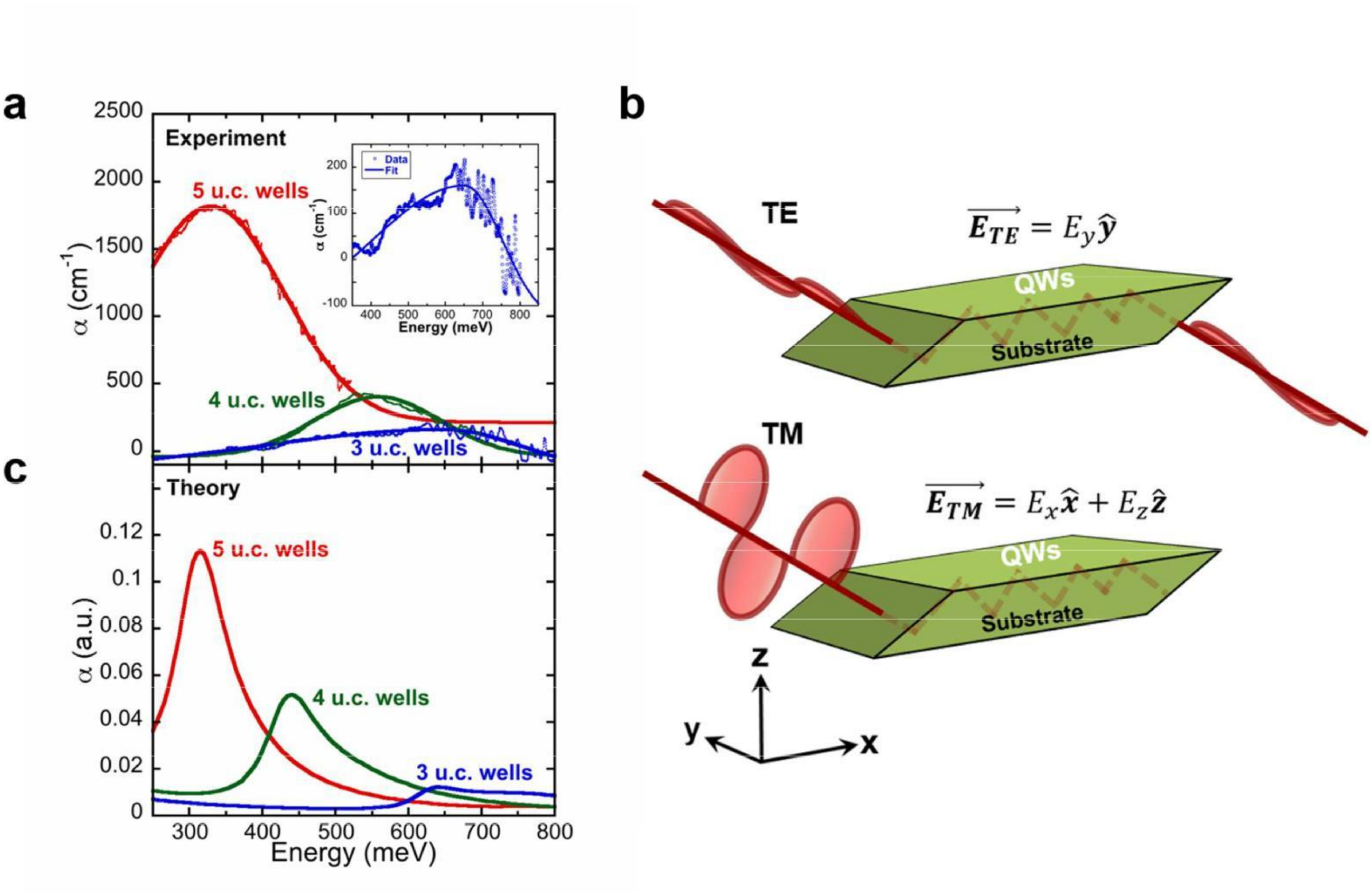

Figure 3. (**a**) Absorption spectra for three-, four- and five-u.c. well samples. The circles are experimental data while the solid lines are Gaussian fits to the data. The calculation of the absorption coefficient in units of cm^{-1} from the raw spectra is discussed in the Supporting Information. Inset: a zoom-in of the absorption peak in the three-u.c. well sample and a bi-Gaussian fit giving the peak energy at ~ 650 meV (see Supporting Information). (**b**) Experimental geometry, indicating the two polarization states used for consecutive measurements. This approach is used to remove the ambiguity as to the origin of any observed absorptions, as intersubband absorption is only stimulated when the optical electric field is perpendicular to the plane of the wells (here, TM). (**c**) Tight binding calculations of the imaginary part of the dielectric function of STO QWs of three-, four-, and five-u.c. widths.

Density functional theory calculations. To further verify the absorption observed in our QW heterostructures is indeed due to the stimulation of intersubband transitions, we performed density functional theory (DFT) calculations on symmetric QW supercells. We model the QW samples using symmetric supercells to avoid the formation of an electric field across the STO wells, as would occur with the use of asymmetric interfaces.[52,53] In the real samples there should be no electric field across the STO wells, as the high electron doping density within the STO would screen an electric field that may arise from the asymmetric interfaces. We vary the supercell composition from $(LAO)_{7.5}/(STO)_{3.5}$ to $(LAO)_{7.5}/(STO)_{5.5}$ in steps of one STO u.c. For ease of comparison with the experimental results, we notate these supercells as three-, four-, and five-u.c. QWs, respectively.

For Ti d_{xy}-derived bands, the dominant bonding is along the x and y directions, while coupling along the z direction is weak. Therefore, if STO is confined in the z direction, the d_{xy} spectrum will be only slightly modified and the change of d_{xy} density of states (DOS) profile is negligible in the QW structure. However, because coupling along the z direction is strong for Ti d_{xz}/d_{yz}-derived bands, the d_{xz}/d_{yz} spectrum will be strongly affected by the confinement. According to tight-binding model analysis,[51] the confinement will give rise to sharp peaks in the d_{xz}/d_{yz} DOS profile. These peaks correspond to different levels of QW states and the number of peaks also depends on STO thickness (*e.g.*, narrower wells can support fewer states than wider wells). Therefore, we only focus on DOS of d_{xz}/d_{yz}-derived bands and compare the energy spacing between sharp peaks to the observed absorption energy. In Figure 4a, we plot the calculated DOS for three-, four-, and five-u.c. QW heterostructures. The energy differences between the ground state and first-excited state peaks in the DOS are 510 meV, 420 meV and 350 meV for three-, four-, and five-u.c. QWs, respectively. DFT results for the five-u.c. QW agree closely with experiment while the calculated energy spacing of the three- and four-u.c. QWs are about 0.1 eV smaller than the observed peaks.

In Figure 4b, we plot the real-space charge density of the QW subbands of a four-u.c. QW. The excess charge is introduced into the STO conduction band automatically *via* the symmetric interfaces, analogous to the *n*-type La doping in the experimental structures. In the figure, the nodal character of each subband is illustrated to the right of each sub-panel, indicating the shape of the corresponding wave function in real space. The nodal structure in our calculations is consistent with wave functions of QW states, with the charge density varying sinusoidally between neighboring Ti atoms. The correspondence between the expected charge density for QW states and the calculated charge density in our structures supports our claim that the sharp states we have calculated in the STO conduction band are indeed the QW states we hope to probe *via* absorption measurements and justifies our interpretation of the spacing between adjacent peaks as the intersubband absorption energy in the real system. With the support of first-principles theory, we can unambiguously ascribe our experimental results to the observation of intersubband transitions in the STO QWs.

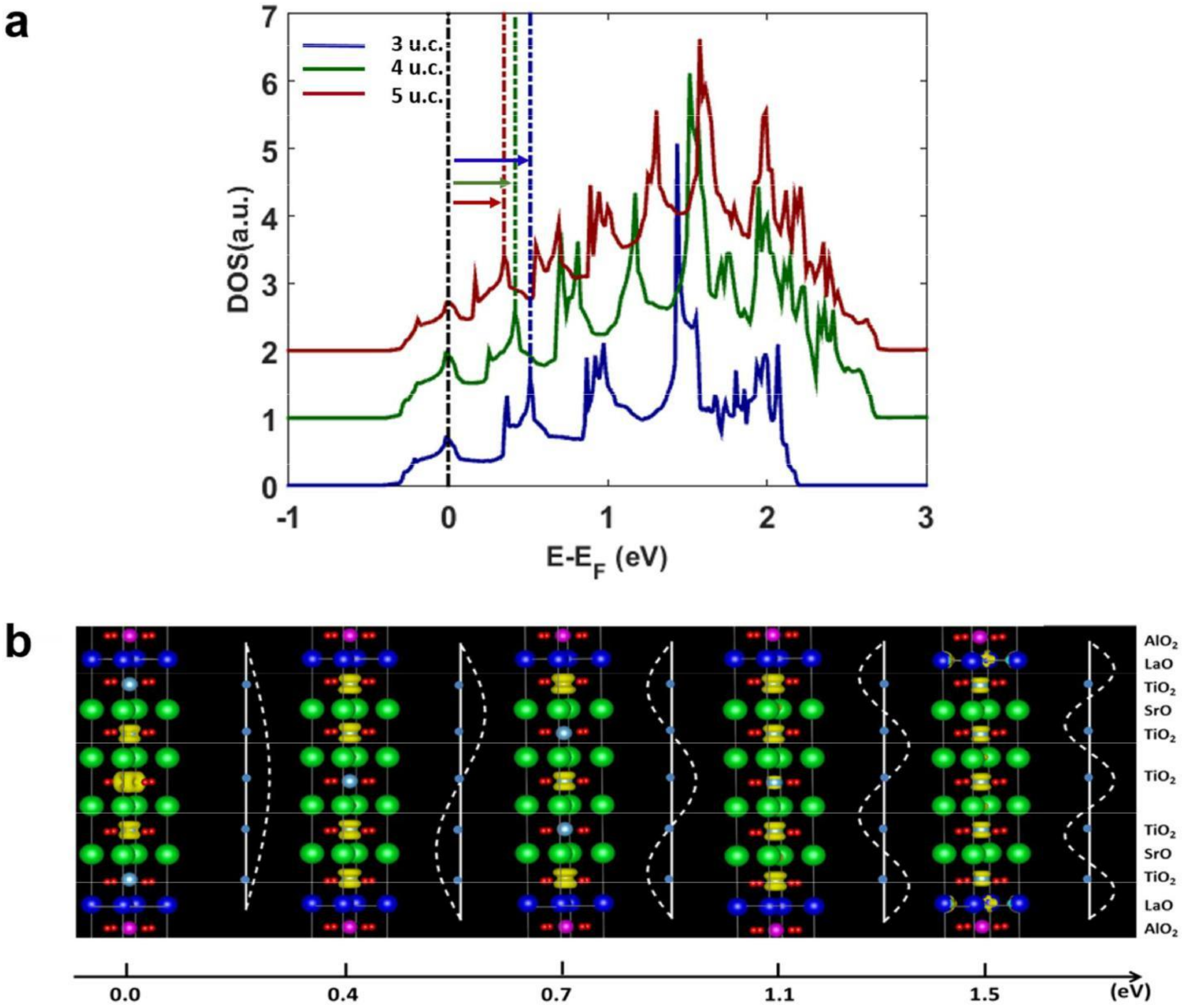

Figure 4. (**a**) The calculated density of states (DOS) displaying the sum of $d_{xz/yz}$ states for three-, four-, and five-u.c. QW structures. The red, green, and blue arrows indicate the transition energy between the ground state and first-excited state in five-, four-, and three-u.c. QWs, respectively. (**b**) Charge distribution in real space corresponding to the five QW subbands in a four-u.c. QW structure. The energy of each state is labeled below the figure. Each plot is accompanied with its schematic wave function on the right. The width of each state is 0.2 eV. La, Al, Sr, Ti, and O atoms are colored as dark blue, magenta, green, light blue and red, respectively.

Conclusions

In summary, we have demonstrated room temperature intersubband absorption in Si-compatible STO/LAO QW heterostructures as well as the ability to modulate the absorption energy by changing the QW width by a single unit cell. The observation of such absorptions can be attributed in large part to the high crystalline quality of our MBE-grown heterostructures. Statistical analysis of STEM intensity mapping indicates that our samples feature interfacial roughness of less than one u.c. on average, while also indicating the unusual feature of symmetric roughness between the *n*- and *p*-type STO/LAO interfaces. The latter feature may be due in part to the introduction of additional charge carriers into the well layers by La doping. Our theoretical calculations are in good agreement with experiment and support our claim that the observed absorptions arise from intersubband transitions of electrons confined in the STO conduction band. Specifically, the calculated energy spacing between QW states is in good agreement with experiment and the calculated spatial distribution of charge within the heterostructures supports the presence of QW states in the STO conduction band. Our results are an important step toward the eventual realization of on-chip TMO QW-based devices that exploit the dozens of emergent phenomena and spontaneous symmetry breaking found in TMO heterostructures.

Methods

Growth of heterostructures. The STO/LAO heterostructures were grown on commercially available double-side polished LAO substrates purchased from MTI Corporation. The substrates were degreased using acetone, isopropanol and deionized water, treated with UV light to remove organic matter on the surface, and then introduced into a DCA 600 MBE system with a base pressure of 5 x 10^{-10} torr. After introduction into the MBE, the substrates were outgassed at 800°C for 20 minutes in an oxygen partial pressure of 5 x 10^{-6} torr to remove any remaining surface contamination. The metal constituents were evaporated from effusion cells and molecular oxygen was used as the oxidant. The metal fluxes were calibrated to be one monolayer (ML)/min using a quartz crystal monitor (QCM), and proper stoichiometry was checked *via in situ* XPS measurements of test samples of STO and LAO grown immediately before fabrication of the heterostructures began. One ML was defined to be one metal atom (Sr, Ti, La, or Al) per (3.79 Å)^2, corresponding to epitaxial growth on cubic LAO. Films were deposited on (001) LAO using a layer-by-layer, alternating shuttering method of Sr and Ti for STO and La and Al for LAO. In the doped STO, the dopant La atoms replaced the corresponding atomic percentage of Sr atoms as controlled by the relative shuttering times of the Sr and La sources.[35] During growth, the substrate was kept at a temperature of 800°C as measured by a thermocouple and the oxygen partial pressure was kept at 5 x 10^{-6} torr. Care was taken to ensure that other gas species present in the chamber were at or below a partial pressure of 1 x 10^{-9} torr during growth, as monitored by *in situ* residual gas mass spectrometry. Once the growth of a heterostructure began, between five and ten well/barrier periods were typically grown during a given growth cycle. Then, the sample was cooled to 200°C in oxygen, removed from the MBE chamber and placed into a UHV transfer line with a base pressure of 3 x 10^{-10} torr without breaking vacuum. Before growing further well/barrier periods on a given sample, the metal fluxes were recalibrated as needed using the QCM and the temperatures of the metal sources adjusted accordingly. In this way, we were able to ensure constant fluxes throughout the growth of the entire heterostructure. The films were monitored during growth by *in situ* RHEED to ensure that the surface crystallinity remained high throughout the entire growth process (see Supporting Information).

STEM and EELS. Z-contrast STEM imaging was performed using Nion UltraSTEM 200 scanning transmission electron microscope operated at 200 kV. Probe convergence angle was 30 mrad, and inner angle of the high angle annular dark field detector was 63 mrad. The images were collected in 20 image stacks and then added using rigid registration to reduce noise. For this imaging technique, the intensity of the atomic columns is roughly proportional to the square of the atomic number Z; therefore, brighter bands correspond to LAO while the darker bands correspond to STO in the images presented herein. Samples were prepared using precision polishing and ion milling.

Infrared spectroscopy. To perform the intersubband absorption measurements, approximately 100 nm of gold were first deposited on both the QW and substrate side of the samples *via* electron-beam evaporation. We then polished the edges of the gold-QW-gold stack at 45 degrees to create two facets for light to enter and exit the sample. The sample was placed in our optical transmission set-up (see Supporting Information) where intersubband absorption spectroscopy is performed by observing the successive transmission spectra of transverse-electric (TE) and transverse-magnetic (TM) light. IR light emitting from our FTIR system is focused into one of the polished edges of each QW sample by a IR-transmissive barium fluoride (BaF_2) lens. The light experiences multiple bounces within the sample as it reflects off the gold layers on either side, and finally emits through the other polished edge. The emitted light is then focused by another BaF_2 lens onto an IR responsive, liquid-nitrogen cooled Mercury-Cadmium-Telluride (MCT) detector. Two measurements were taken for each sample, one with TE-polarized incident light, and one with TM-polarized light, with the discrimination occurring *via* employment of a zinc-selenide (ZnSe) linear polarizer placed in between the first lens and the sample.

Theoretical calculations. *Tight-binding:* The details of the tight-binding (TB) simulations can be found in our previous work.[51] Following the notations in Lin *et al.*,[51] the non-zero TB parameters are = 4.0 , , = 1.5 , and , = 0.3 . The temperature is 300 K, and the chemical potential is chosen to be 4 eV, corresponding to about 1 at% electron doping. The imaginary part of the dielectric function, corresponding to the light absorption, is plotted in Fig. 3c. The TB parameters used here are consistent with the ellipsometry measurement of bulk STO given by Zollner *et al.*[54]

Density functional theory: First principle calculations based on density functional theory (DFT) were performed using local-density approximation (LDA)[55] for the projector-augmented-wave pseudopotentials,[56] as implemented in the Vienna Ab-Initio Simulation Package code.[57] For Sr, Ti, La, Al and O, $4s^24p^65s^2$, $3s^23p^64s^23d^2$, $5s^25p^65d^16s^2$, $2s^22p^1$ and $2s^22p^4$ are included, respectively. The plane-wave cutoff energy was 700 eV. $(LAO)_{7.5}/(STO)_{4.5}$ supercell was employed and symmetric TiO_2/LaO (*n*-type) interfaces were adopted. Consistent with experiment, we used the theoretical a_{LAO} = 3.74 Å as the in-plane lattice constant. All atom positions were fully relaxed until residual forces were less than 0.01 eV Å^{-1}. For self-consistent calculation, we sampled the Brillouin zone with 8 × 8 × 1 Monkhorst-Pack *k*-point grids[58] and we used 16 × 16 × 1 Kmesh for the accurate density of states calculation. As explained in the main manuscript, we only focus on the $d_{xz/yz}$-derived bands in the DFT analysis presented in the "Density functional theory calculations" section and in Figure 4.

Acknowledgments

The authors thank Rik Dey, Sarmita Majumder, and Sanjay Banerjee of the Microelectronics Research Center at the University of Texas at Austin for performing in-plane transport measurements. JEO is grateful for the generous support of the National Science Foundation Graduate Research Fellowship under Grant No. DGE-1610403. The work at the University of Texas is supported by the Air Force Office of Scientific Research under Grant FA9550–12–10494, through Scientific Discovery through Advanced Computing (SciDAC) program funded by U.S. Department of Energy, Office of Science, Advanced Scientific Computing Research and Basic Energy Sciences under award number DESC0008877 and by the Texas Advanced Computing Center. Electron microscopy work (Q. He and A. Borisevich) was supported by the U.S. Department of Energy (DOE) Office of Science, Office of Basic Energy Sciences (BES), Materials Science and Engineering Division.

Supporting Information. The Supporting Information file contains additional details on the structural, optical, and electrical characterization of the STO/LAO QW heterostructures discussed herein. The Supplementary Information is available online.

References

(1) Li, L.; Richter, C.; Mannhart, J.; Ashoori, R. C. Coexistence of Magnetic Order and Two-Dimensional Superconductivity at $LaAlO_3/SrTiO_3$ Interfaces. *Nat. Phys.* **2011**, *7*, 762– 766.

(2) Bert, J. A.; Kalisky, B.; Bell, C.; Kim, M.; Hikita, Y.; Hwang, H. Y.; Moler, K. A. Direct Imaging of the Coexistence of Ferromagnetism and Superconductivity at the $LaAlO_3/SrTiO_3$ Interface. *Nat. Phys.* **2011**, *7*, 767–771.

(3) Reyren, N.; Thiel, S.; Caviglia, A. D.; Kourkoutis, L. F.; Hammerl, G.; Richter, C.; Schneider, C. W.; Kopp, T.; Rüetschi, A.-S.; Jaccard, D.; Gabay, M.; Muller, D. A.; Triscone, J.-M.; Mannhart, J. Superconducting Interfaces Between Insulating Oxides. *Science (80-.).* **2007**, *317*.

(4) Lee, J.-S.; Xie, Y. W.; Sato, H. K.; Bell, C.; Hikita, Y.; Hwang, H. Y.; Kao, C.-C. Titanium d_{xy} Ferromagnetism at the $LaAlO_3/SrTiO_3$ Interface. *Nat. Mater.* **2013**, *12*, 703– 706.

(5) Kalisky, B.; Bert, J. A.; Klopfer, B. B.; Bell, C.; Sato, H. K.; Hosoda, M.; Hikita, Y.; Hwang, H. Y.; Moler, K. A. Critical Thickness for Ferromagnetism in $LaAlO_3/SrTiO_3$ Heterostructures. *Nat. Commun.* **2012**, *3*, 922.

(6) Brinkman, A.; Huijben, M.; van Zalk, M.; Huijben, J.; Zeitler, U.; Maan, J. C.; van der

Wiel, W. G.; Rijnders, G.; Blank, D. H. A.; Hilgenkamp, H. Magnetic Effects at the Interface between Non-Magnetic Oxides. *Nat. Mater.* **2007**, *6*, 493–496.

(7) Ohtomo, A.; Hwang, H. Y. A High-Mobility Electron Gas at the $LaAlO_3/SrTiO_3$ Heterointerface. *Nature* **2004**, *427*, 423–426.

(8) Biscaras, J.; Bergeal, N.; Kushwaha, A.; Wolf, T.; Rastogi, A.; Budhani, R. C.; Lesueur, J. Two-Dimensional Superconductivity at a Mott Insulator/Band Insulator Interface $LaTiO_3/SrTiO_3$. *Nat. Commun.* **2010**, *1*, 1–5.

(9) Hwang, H. Y.; Iwasa, Y.; Kawasaki, M.; Keimer, B.; Nagaosa, N.; Tokura, Y. Emergent Phenomena at Oxide Interfaces. *Nat. Mater.* **2012**, *11*, 103–113.

(10) Okamoto, S.; Millis, A. J. Electronic Reconstruction at an Interface between a Mott Insulator and a Band Insulator. *Nature* **2004**, *428*, 630–633.

(11) Doennig, D.; Pentcheva, R. Control of Orbital Reconstruction in $(LaAlO3)_M/(SrTiO3)_N$ (001) Quantum Wells by Strain and Confinement. *Sci. Rep.* **2015**, *5*, 7909.

(12) Huijben, M.; Rijnders, G.; Blank, D. H. A.; Bals, S.; Aert, S. Van; Verbeeck, J.; Tendeloo, G. Van; Brinkman, A.; Hilgenkamp, H. Electronically Coupled Complementary Interfaces between Perovskite Band Insulators. *Nat. Mater.* **2006**, *5*, 556–560.

(13) Chakhalian, J.; Freeland, J. W.; Millis, A. J.; Panagopoulos, C.; Rondinelli, J. M. *Colloquium*: Emergent Properties in Plane View: Strong Correlations at Oxide Interfaces. *Rev. Mod. Phys.* **2014**, *86*, 1189–1202.

(14) McKee, R. A.; Walker, F. J.; Conner, J. R.; Specht, E. D.; Zelmon, D. E. Molecular Beam Epitaxy Growth of Epitaxial Barium Silicide, Barium Oxide, and Barium Titanate on Silicon. *Appl. Phys. Lett.* **1991**, *59*, 782–784.

(15) Park, J. W.; Bogorin, D. F.; Cen, C.; Felker, D. A.; Zhang, Y.; Nelson, C. T.; Bark, C. W.; Folkman, C. M.; Pan, X. Q.; Rzchowski, M. S.; Levy, J.; Eom, C. B. Creation of a Two-Dimensional Electron Gas at an Oxide Interface on Silicon. *Nat. Commun.* **2010**, *1*, 94.

(16) Ponath, P.; Fredrickson, K.; Posadas, A. B.; Ren, Y.; Wu, X.; Vasudevan, R. K.; Baris Okatan, M.; Jesse, S.; Aoki, T.; McCartney, M. R.; Smith, D. J.; Kalinin, S. V.; Lai, K.; Demkov, A. A. Carrier Density Modulation in a Germanium Heterostructure by Ferroelectric Switching. *Nat. Commun.* **2015**, *6*, 6067.

(17) Mannhart, J.; Schlom, D. G. Oxide Interfaces--An Opportunity for Electronics. *Science (80-.).* **2010**, *327*, 1607–1611.

(18) Bogorin, D. F.; Irvin, P.; Cen, C.; Levy, J. $LaAlO_3/SrTiO_3$-Based Device Concepts. In *Multifunctional Oxide Heterostructures*; Oxford University Press, 2012; pp. 364–388.

(19) Bjaalie, L.; Himmetoglu, B.; Weston, L.; Janotti, A.; Van de Walle, C. G. Oxide Interfaces for Novel Electronic Applications. *New J. Phys.* **2014**, *16*, 025005.

(20) Abel, S.; Stöferle, T.; Marchiori, C.; Rossel, C.; Rossell, M. D.; Erni, R.; Caimi, D.; Sousa, M.; Chelnokov, A.; Offrein, B. J.; Fompeyrine, J. A Strong Electro-Optically Active Lead-Free Ferroelectric Integrated on Silicon. *Nat. Commun.* **2013**, *4*, 1671.

(21) Robertson, J. Band Offsets of Wide-Band-Gap Oxides and Implications for Future Electronic Devices. *J. Vac. Sci. Technol. B Microelectron. Nanom. Struct.* **2000**, *18*, 1785–1791.

(22) Pereira, T. A. S.; Bezerra, M. G.; Freire, J. A. K.; Freire, V. N.; Farias, G. A. Energy Levels in Si and $SrTiO_3$-Based Quantum Wells with Charge Image Effects. *Brazilian J. Phys.* **2006**, *36*, 347–349.

(23) Capasso, F.; Sirtori, C.; Cho, A. Y. Coupled Quantum Well Semiconductors with Giant Electric Field Tunable Nonlinear Optical Properties in the Infrared. *IEEE J. Quantum*

Electron. **1994**, *30*, 1313–1326.

(24) Jackson, C. A.; Stemmer, S. Interface-Induced Magnetism in Perovskite Quantum Wells. *Phys. Rev. B* **2013**, *88*.

(25) Need, R. F.; Isaac, B. J.; Kirby, B. J.; Borchers, J. A.; Stemmer, S.; Wilson, S. D. Interface-Driven Ferromagnetism within the Quantum Wells of a Rare Earth Titanate Superlattice. *Phys. Rev. Lett.* **2016**, *117*, 037205.

(26) Jiang, J. C.; Pan, X. Q.; Tian, W.; Theis, C. D.; Schlom, D. G. Abrupt $PbTiO_3/SrTiO_3$ Superlattices Grown by Reactive Molecular Beam Epitaxy. *Appl. Phys. Lett.* **1999**, *74*, 2851–2853.

(27) Kanno, I.; Hayashi, S.; Takayama, R.; Hirao, T. Superlattices of $PbZrO_3$ and $PbTiO_3$ Prepared by Multi-Ion-Beam Sputtering. *Appl. Phys. Lett.* **1996**, *68*, 328–330.

(28) Choi, T.; Lee, J. Structural and Dielectric Properties of Artificial $PbZrO_3/PbTiO_3$ Superlattices Grown by Pulsed Laser Deposition. *Thin Solid Films* **2005**, *475*, 283–286.

(29) Bousquet, E.; Dawber, M.; Stucki, N.; Lichtensteiger, C.; Hermet, P.; Gariglio, S.; Triscone, J.-M.; Ghosez, P. Improper Ferroelectricity in Perovskite Oxide Artificial Superlattices. *Nature* **2008**, *452*, 732–736.

(30) Dawber, M.; Lichtensteiger, C.; Cantoni, M.; Veithen, M.; Ghosez, P.; Johnston, K.; Rabe, K. M.; Triscone, J.-M. Unusual Behavior of the Ferroelectric Polarization in $PbTiO_3/SrTiO_3$ Superlattices. *Phys. Rev. Lett.* **2005**, *95*, 177601.

(31) Zhao, K.; Chen, G.; Li, B.-S.; Shen, A. Mid-Infrared Intersubband Absorptions in ZnO/ZnMgO Multiple Quantum Wells. *Appl. Phys. Lett.* **2014**, *104*, 212104.

(32) Choi, M.; Lin, C.; Butcher, M.; Rodriguez, C.; He, Q.; Posadas, A. B.; Borisevich, A. Y.; Zollner, S.; Demkov, A. A. Quantum Confinement in Transition Metal Oxide Quantum Wells. *Appl. Phys. Lett.* **2015**, *106*, 192902.

(33) Batey, J.; Wright, S. L. Energy Band Alignment in GaAs:(Al,Ga)As Heterostructures: The Dependence on Alloy Composition. *J. Appl. Phys.* **1986**, *59*, 200–209.

(34) Nakagawa, N.; Hwang, H. Y.; Muller, D. A. Why Some Interfaces Cannot Be Sharp. *Nat. Mater.* **2006**, *5*, 204–209.

(35) Choi, M.; Posadas, A. B.; Rodriguez, C. A.; O'Hara, A.; Seinige, H.; Kellock, A. J.; Frank, M. M.; Tsoi, M.; Zollner, S.; Narayanan, V.; Demkov, A. A. Structural, Optical, and Electrical Properties of Strained La-Doped $SrTiO_3$ Films. *J. Appl. Phys.* **2014**, *116*, 043705.

(36) Son, J.; Moetakef, P.; Jalan, B.; Bierwagen, O.; Wright, N. J.; Engel-Herbert, R.; Stemmer, S. Epitaxial $SrTiO_3$ Films with Electron Mobilities Exceeding 30,000 Cm^2 V^{-1} s^{-1}. *Nat. Mater.* **2010**, *9*, 482–484.

(37) Segovia, P.; Michel, E. G.; Ortega, J. E. Quantum Well States and Interface Quality in Cu/Co(100)/Cu(100) System. *Surf. Sci.* **1998**, *402404*, 377–381.

(38) Singh, J.; Bajaj, K. K.; Chaudhuri, S. Theory of Photoluminescence Line Shape Due to Interfacial Quality in Quantum Well Structures. *Appl. Phys. Lett.* **1984**, *44*, 805–807.

(39) Singh, J.; Bajaj, K. K. Role of Interface Roughness and Alloy Disorder in Photoluminescence in Quantum-Well Structures. *J. Appl. Phys.* **1985**, *57*, 5433–5437.

(40) Willmott, P. R.; Pauli, S. A.; Herger, R.; Schlepütz, C. M.; Martoccia, D.; Patterson, B. D.; Delley, B.; Clarke, R.; Kumah, D.; Cionca, C.; Yacoby, Y. Structural Basis for the Conducting Interface between $LaAlO_3$ and $SrTiO_3$. *Phys. Rev. Lett.* **2007**, *99*, 155502.

(41) Qiao, L.; Droubay, T. C.; Shutthanandan, V.; Zhu, Z.; Sushko, P. V; Chambers, S. A. Thermodynamic Instability at the Stoichiometric $LaAlO_3/SrTiO_3$ (001) Interface. *J. Phys.*

Condens. Matter **2010**, *22*, 312201.

(42) Yamamoto, R.; Bell, C.; Hikita, Y.; Hwang, H. Y.; Nakamura, H.; Kimura, T.; Wakabayashi, Y. Structural Comparison of *n*-Type and *p*-Type $LaAlO_3/SrTiO_3$ Interfaces. *Phys. Rev. Lett.* **2011**, *107*, 036104.

(43) Zhong, Z.; Xu, P. X.; Kelly, P. J. Polarity-Induced Oxygen Vacancies at $LaAlO_3/SrTiO_3$ Interfaces. *Phys. Rev. B* **2010**, *82*, 165127.

(44) Lee, J.; Demkov, A. A. Charge Origin and Localization at the *n*-Type $SrTiO_3/LaAlO_3$ Interface. *Phys. Rev. B* **2008**, *78*, 193104.

(45) Helm, M. Chapter 1 The Basic Physics of Intersubband Transitions. *Semicond. Semimetals* **1999**, *62*, 1–99.

(46) Coon, D. D.; Karunasiri, R. P. G. New Mode of IR Detection Using Quantum Wells. *Appl. Phys. Lett.* **1984**, *45*, 649–651.

(47) Liu, H. C.; Buchanan, M.; Wasilewski, Z. R. How Good Is the Polarization Selection Rule for Intersubband Transitions? *Appl. Phys. Lett.* **1998**, *72*, 1682–1684.

(48) Sirenko, A. A.; Bernhard, C.; Golnik, A.; Clark, A. M.; Hao, J.; Si, W.; Xi, X. X. Soft-Mode Hardening in $SrTiO_3$ Thin Films. *Nature* **2000**, *404*, 373–376.

(49) Willett-Gies, T.; DeLong, E.; Zollner, S. Vibrational Properties of Bulk $LaAlO_3$ from Fourier-Transform Infrared Ellipsometry. *Thin Solid Films* **2014**, *571*, 620–624.

(50) Santander-Syro, A. F.; Copie, O.; Kondo, T.; Fortuna, F.; Pailhès, S.; Weht, R.; Qiu, X. G.; Bertran, F.; Nicolaou, A.; Taleb-Ibrahimi, A.; Le Fèvre, P.; Herranz, G.; Bibes, M.; Reyren, N.; Apertet, Y.; Lecoeur, P.; Barthélémy, A.; Rozenberg, M. J. Two-Dimensional Electron Gas with Universal Subbands at the Surface of $SrTiO_3$. *Nature* **2011**, *469*, 189–193.

(51) Lin, C.; Posadas, A.; Choi, M.; Demkov, A. A. Optical Properties of Transition Metal Oxide Quantum Wells. *J. Appl. Phys.* **2015**, *117*, 034304.

(52) Park, M. S.; Rhim, S. H.; Freeman, A. J. Charge Compensation and Mixed Valency in $LaAlO_3/SrTiO_3$ Heterointerfaces Studied by the FLAPW Method. *Phys. Rev. B* **2006**, *74*, 205416.

(53) Bristowe, N. C.; Artacho, E.; Littlewood, P. B. Oxide Superlattices with Alternating *p* and *n* Interfaces. *Phys. Rev. B* **2009**, *80*, 045425.

(54) Zollner, S.; Demkov, A. A.; Liu, R.; Fejes, P. L.; Gregory, R. B.; Alluri, P.; Curless, J. A.; Yu, Z.; Ramdani, J.; Droopad, R.; Tiwald, T. E.; Hilfiker, J. N.; Woollam, J. A. Optical Properties of Bulk and Thin-Film $SrTiO_3$ on Si and Pt. *J. Vac. Sci. Technol. B Microelectron. Nanom. Struct.* **2000**, *18*, 2242–2254.

(55) Perdew, J. P.; Zunger, A. Self-Interaction Correction to Density-Functional Approximations for Many-Electron Systems. *Phys. Rev. B* **1981**, *23*, 5048–5079.

(56) Blöchl, P. E. Projector Augmented-Wave Method. *Phys. Rev. B* **1994**, *50*, 17953–17979.

(57) Kresse, G.; Furthmüller, J. Efficient Iterative Schemes for *Ab Initio* Total-Energy Calculations Using a Plane-Wave Basis Set. *Phys. Rev. B* **1996**, *54*, 11169–11186.

(58) Monkhorst, H. J.; Pack, J. D. Special Points for Brillouin-Zone Integrations. *Phys. Rev. B* **1976**, *13*, 5188–5192.

For Table of Contents Only